

Extending a UGV Teleoperation FLC Interface with Wireless Network Connectivity Information

Sergio Caccamo, Ramviyas Parasuraman, Fredrik Båberg, Petter Ögren

Abstract— Teleoperated Unmanned Ground Vehicles (UGVs) are expected to play an important role in future search and rescue operations. In such tasks, two factors are crucial for a successful mission completion: operator situational awareness and robust network connectivity between operator and UGV. In this paper, we address both these factors by extending a new Free Look Control (FLC) operator interface with a graphical representation of the Radio Signal Strength (RSS) gradient at the UGV location. We also provide a new way of estimating this gradient using multiple receivers with directional antennas. The proposed approach allows the operator to stay focused on the video stream providing the crucial situational awareness, while controlling the UGV to complete the mission without moving into areas with dangerously low wireless connectivity.

The approach is implemented on a KUKA youBot using commercial-off-the-shelf components. We provide experimental results showing how the proposed RSS gradient estimation method performs better than a difference approximation using omnidirectional antennas and verify that it is indeed useful for predicting the RSS development along a UGV trajectory. We also evaluate the proposed combined approach in terms of accuracy, precision, sensitivity and specificity.

I. INTRODUCTION

Today, Unmanned Ground Vehicles (UGVs)¹ play an increasingly important role in several applications, such as Urban Search And Rescue (USAR), Explosive Ordinance Disposal (EOD), reconnaissance and inspections of disaster areas. In such missions, the operator needs robust wireless network connectivity not to lose control of the UGV, and a good situational awareness in order to decide what to do.

The importance of connectivity was made evident during a radiation survey mission at Fukushima, when the robot Quince was disconnected from the operator due to cable breakage, and was subsequently abandoned at the site [1]. Wireless channels are a natural alternative to cables, but present other challenges, such as shadowing or multipath fading, radio signal propagation effects that are difficult to predict, leading to low (or no) connectivity regions scattered throughout the environment [2], [3]. While increased autonomy in robots could solve some of the problems of low wireless connectivity [4], teleoperation of robots is still needed in many situations, since humans are still far more versatile than autonomous systems, especially in unknown and unpredictable environments [5], [6].

The authors are with the Computer Vision and Active Perception Lab., Centre for Autonomous Systems, School of Computer Science and Communication, Royal Institute of Technology (KTH), SE-100 44 Stockholm, Sweden. e-mail: {caccamo|ramviyas|fbaberg|petter}@kth.se

The authors gratefully acknowledge funding from the European Union's seventh framework program (FP7), under grant agreement FP7-ICT-609763 TRADR.

¹We will use the terms UGV and robot interchangeably in this paper.



Fig. 1: A youBot mobile robot equipped with wireless network hardware used in the experiments. The directional antennas are visible in the corners of the youBot, and the omnidirectional antenna for communication in the center.

Another important aspect in USAR missions is the situational awareness. A number of studies have been addressing the subject, and it turns out that a significant amount of the UGV mission time is devoted to improving the operator situational awareness. In fact, the fraction of mission time spent on improving situational awareness was estimated to as much as 49% in [7] and to roughly 30% in [8]. Furthermore, [9] concluded that most of the critical incidents in the investigated USAR competition were due to lacking situation awareness. The challenge addressed in this paper is how to add the crucial awareness of network connectivity to the operator, without disturbing the normal (spatial) situational awareness. We do this by combining the Free Look Control (FLC) interface proposed in [10] with ideas regarding wireless information from [11], [12], and validate the approach using the UGV in Figure 1.

FLC is an interface borrowed from the computer gaming community, where it is used in so-called First Person Shooter (FPS) games, such as Halo, Half-Life, and Call of Duty [13]. The interface allows the operator to ignore the orientation of the UGV chassis, and completely focus on commands for moving the UGV camera through the remote environment.

In this paper we continue to take inspiration from the gaming world, and now look at how the gamer is made aware

of something happening around him/her. If a game character is hurt from behind, the bottom part of a circle surrounding the center of the screen flashes red. Similarly, if the character is hurt from the right side, the right part of the circle flashes red. Using similar ideas, we extend the FLC interface with a colored frame surrounding the camera view. The undesirable motion direction, from a network connectivity point of view, is now shown by coloring the corresponding part of the frame red. This is combined with a tactile vibration feedback when the threshold is close to being reached. We believe that this approach of combining more abstract signal strength gradient information with spatial situational awareness will work as well for UGV teleoperation, as it has done regarding changes in health level in the world of computer games.

The approach described above goes beyond the standard way of presenting the Radio Signal Strength (RSS), which is a signal strength indicator of the same type as the ones used to convey network status or battery level in most mobile phones today. To enable the new interface, we also need a reliable estimate of the gradient of the RSS, which provides the Direction of Arrival (DoA) information. This is done using a new hardware configuration, inspired by [11], [12], shown in Figure 1.

The main contributions of this paper can be summarized as:

- 1) we propose a new way of estimating RSS gradients using receiver spatial diversity with directional antennas;
- 2) we propose an extension of the FLC interface to include the RSS gradient estimates, enabling the operator to improve his situational awareness.

The outline of the paper is as follows. Section II presents the related work, followed by a description of the proposed methodology in Section III. Experiments validating the approach, performed indoor in both line-of-sight (LOS) and non line-of-sight (NLOS) conditions are detailed in Section IV. The results are presented in Section V and finally conclusions and future work are discussed in Section VI.

II. RELATED WORK

Today, almost all teleoperated UGVs are equipped with cameras transmitting the live video feed to the operators Human Machine Interface (HMI) at a remote control station. A lot of work has been devoted to the HMI design to increase the situational awareness. For instance, in a study of operator control units based on experiences from the AAAI Robot Rescue Competitions in 2002-2004 [14], the authors noticed an evolution over time, towards a large single interface, with a large percentage of the screen dedicated to video.

A study conducted using response robots after the World Trade Center disaster has shown why it is essential to have a robust and stable wireless connection between the robot and the operator [2]. While some studies promote alternative and hybrid communication strategies [15], [16], [17], [12], there has been a very limited amount of research done in presenting the wireless connectivity information to the operator in an intuitive manner. In [11], a haptic device

was used to provide feedback on wireless signal strength surrounding the robot. However, the HMI does not always include a haptic feedback device and hence using the visual interface is worth considering. To the best of our knowledge, this has not yet been explored in the literature.

The use of RSS gradients in radio source seeking or source localization has shown promising results in [12], [18], [19]. Measuring the RSS around the robot helps in estimating the RSS gradients which provide the DoA of radio signals at the robot location. There are several methods to estimate the RSS gradients, such as rotating directional antennas [20], [16], measurements at various positions in a specific manner [18], [19], and multiple receivers exploiting receiver diversity [12], [21]. Besides, it is shown in [21] that estimating the RSS gradients using receiver diversity outperforms antenna diversity approaches because of two reasons: low temporal influence in the RSS measurements and advantages such as reduced hardware complexity and energy needs (e.g. no rotating antennas), reduced overhead time in scanning for measurements, etc. In addition, [21] investigated various receiver placements on a robot for determining the RSS gradients and it is reported that the receivers (or antennas of receivers) placed on the corners of the robot resulted in better performance, and hence we retain this receiver configuration in this work.

In this paper, we propose a spatial-diversity method building upon the successful approaches used in [12], [11] to estimate the RSS gradients. However, we go beyond [12], [11] and apply directional antennas to each of the wireless receivers instead of omnidirectional antennas to increase the accuracy of the DoA estimation. Thus, the method proposed here (for the robot), and the active antenna tracking approach used in [16] (at the operator control station), are complementary ways of improving the end-to-end throughput of the wireless network. Furthermore, this paper transcends [10] by extending the FLC control mode with network connectivity information, and verifying that the DoA estimates does indeed give reliable information of the development of the RSS level.

III. PROPOSED APPROACH

In this section we present the proposed approach for improving operator situation awareness, including network connectivity awareness. First we describe the signal processing part (DoA estimation) of the approach. Then we describe the FLC control interface suggested in [10]. Finally, we describe the new HMI combining the above two components.

A. Radio signal strength DoA estimation

The Shannon-Hamilton theorem [22] states that the RSS received at a wireless receiver has direct impact on the network capacity (throughput) ($C \propto \log(1 + 10^{\frac{RSS - Noise}{10}})$), thereby permitting the RSS measure (in dB) as an indication of the network connectivity. The RSS can be modeled with

the following equation:

$$RSS = \underbrace{RSS_{d_0} - 10\eta \log_{10}\left(\frac{d}{d_0}\right)}_{\text{deterministic}} - \underbrace{\Psi(d) - \Omega(d, t)}_{\text{stochastic}}; \quad (1)$$

where RSS_{d_0} is the RSS at a reference distance (d_0), η is the propagation constant of the environment, d is the distance of the receiver from the radio source, Ψ is a stochastic (gaussian) variable representing (spatial) shadowing effects caused by the objects in the environment, and Ω is another stochastic variable in the RSS representing (spatial and temporal) multipath fading effects and dynamics in the environment [3]. The stochastic variations in the RSS can be mitigated by using a combination of filters and antenna diversity technique provided that the antenna spacing is far enough ($6 \text{ cm} \leq \Delta \leq 15 \text{ cm}$ for 2.4 GHz signal [3]) to experience uncorrelated fading. This fosters the use of RSS gradient-based approaches in robots.

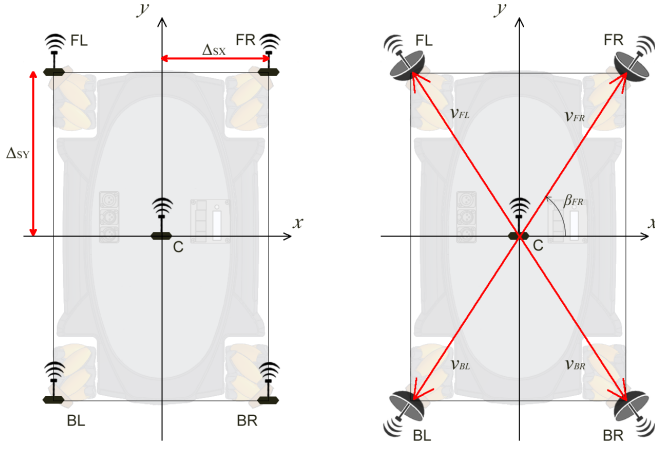


Fig. 2: Configuration of wireless adapters with (a) omnidirectional and (b) directional antennas surrounding the robot.

We propose the planar squared receiver configurations [21] in Figure 2 with either omnidirectional (left) or directional (right) antenna configurations. These configurations rely on the distances between antennas and on the differences between RSS magnitudes for obtaining RSS gradients. Modeling the RSS as a scalar field ($\Gamma(x) : \mathbb{R}^3 \rightarrow \mathbb{R}$), the above mentioned configurations permits to obtain an indirect estimation of the gradient (spatial derivative) of the RSS field. In the omnidirectional receivers configuration, the following finite difference formula [21] is applied on the RSS measurements from the Front-Right (FR), Front-Left (FL), Back-Right (BR), Back-Left (BL) receivers to obtain the RSS gradient vector $\vec{V}_f = [V_{f_x}, V_{f_y}]$, where

$$\begin{aligned} V_{f_x} &= \frac{(FR - FL)}{2\Delta_{sx}} + \frac{(BR - BL)}{2\Delta_{sx}}, \\ V_{f_y} &= \frac{(FR - BR)}{2\Delta_{sy}} + \frac{(FL - BL)}{2\Delta_{sy}}, \end{aligned} \quad (2)$$

and Δ_{sx} , Δ_{sy} are the spatial separation between antennas.

In the second configuration with directional antennas at the receivers, we use direct vector addition to obtain the DoA

and use it as an RSS gradient estimate as follows:

$$\vec{V}_f = \widehat{V}_{FR}FR + \widehat{V}_{FL}FL + \widehat{V}_{BR}BR + \widehat{V}_{BL}BL \quad (3)$$

where \widehat{V}_{FR} , \widehat{V}_{FL} , \widehat{V}_{BR} and \widehat{V}_{BL} are unit vectors in the directions of the different sensors from the center of the UGV, as shown in Figure 2. This configuration relies on a weighted sum of vectors whose magnitudes are amplified by the RSS measurements from the respective receivers. Each antenna is oriented in the direction of its correspondent placement vector. Note that we are only interested in the direction of the estimate, not the magnitude. Thus we disregard the fact that the two estimates above have different magnitudes (and units).

Although we apply equation (3) in the second configuration, the finite difference method in equation (2) can also be used to estimate the RSS gradients as shown in [17]. Therefore it is possible to employ redundant schemes for computing RSS gradients so that device failures or misreadings can be tolerated to some extent (as discussed in [12]). Proving this fault-tolerance ability is beyond the scope of this paper, but will be included in future works.

The DoA of the radio signal is obtained from the RSS gradients as,

$$\text{DoA} = \tan^{-1}\left(\frac{V_{f_y}}{V_{f_x}}\right). \quad (4)$$

The two configurations share a common central point constituted by a central receiver with an omnidirectional antenna. The communication with the radio transmitter (source), which host the controller station, goes through the central receiver whereas the others receivers, even though connected to the radio source, are passive and only used for the RSS gradient estimation in this paper. We conduct experiments to verify the best configuration among the above two in Section IV.

B. Free Look Control (FLC)

In this section, we will describe the new FLC control mode, and compare it to Tank Control (TC), the control mode used in most UGVs today [10]. In TC, camera and robot platform controls are decoupled, requiring the user to mentally keep track of at least two angles while teleoperating an UGV: the camera angle relative to the UGV, and the platform orientation with respect to the world frame. In contrast, FLC couples both camera and platform control (while decoupling the orientation and translation) and thereby only requires the user to choose the desired direction of camera movement [10]. This makes FLC the most suitable control modality for the connectivity aware method we propose in this paper.

As in FPS video games, FLC commands are interpreted in relation to the camera view, moving forward means moving in the direction the camera is facing etc. A mathematical description of the FLC mode is provided below. We first define the kinematic movement of a general differential drive

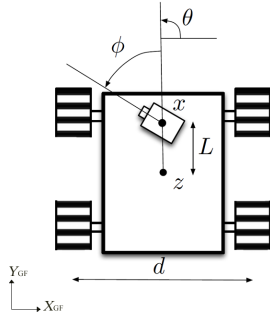


Fig. 3: A general differential drive robot mounted with a camera.

robot, see Figure 3, as in Equation (5) below.

$$\begin{aligned}
 \dot{z}_1 &= \frac{v_r + v_l}{2} \cos \theta, \\
 \dot{z}_2 &= \frac{v_r + v_l}{2} \sin \theta, \\
 \dot{\theta} &= \frac{v_r - v_l}{d}, \\
 \dot{\phi} &= k,
 \end{aligned} \tag{5}$$

where $z = (z_1, z_2)$ and $x = (x_1, x_2)$ are respectively the positions of the robot and camera in the global frame (GF), θ and ϕ are the orientations of the robot (in the GF) and the camera (relative to the robot), v_r, v_l are velocities of the right and left wheels/tracks respectively, d is the width of the vehicle, L is the distance between the camera center and the robot center, and k is the angular velocity of the camera relative to the robot. Note that the youBot in Figure 1 is not differential drive, but many search and rescue robots are, thus we treat that case here, and let the youBot emulate such a case.

Remember that the objective of the FLC mode is to combine the control of platform and the camera in such a way that the orientation and translation inputs are separated. This means that the resulting FLC kinematics should resemble the FPS control shown in Equation (6) (in our case, the camera corresponds to the FPS character).

$$\begin{aligned}
 \begin{pmatrix} \dot{x}_1 \\ \dot{x}_2 \end{pmatrix} &= \begin{pmatrix} \cos \psi & -\sin \psi \\ \sin \psi & \cos \psi \end{pmatrix} \begin{pmatrix} v_x \\ v_y \end{pmatrix}, \\
 \dot{\psi} &= \omega,
 \end{aligned} \tag{6}$$

where (x_1, x_2) and $\psi = \theta + \phi$ are position and orientation of the camera (FPS character), v_x and v_y are the inputs from the gamepad, to represent front/back and left/right motions respectively, and ω is the orientation input to the camera provided from the gamepad.

This conversion (from Equation (5) to Equation (6)) is realized by applying a control model shown in Equation (7) that maps the user inputs (v_x, v_y, ω) to the kinematic inputs (v_r, v_l, k) . More detailed description and proofs are in [10].

$$\begin{aligned}
 \begin{pmatrix} v_l \\ v_r \end{pmatrix} &= \begin{pmatrix} 1/2 & 1/2 \\ -L/d & L/d \end{pmatrix}^{-1} \begin{pmatrix} \cos \phi & -\sin \phi \\ \sin \phi & \cos \phi \end{pmatrix} \begin{pmatrix} v_x \\ v_y \end{pmatrix}, \\
 k &= \omega - \frac{v_r - v_l}{d},
 \end{aligned} \tag{7}$$

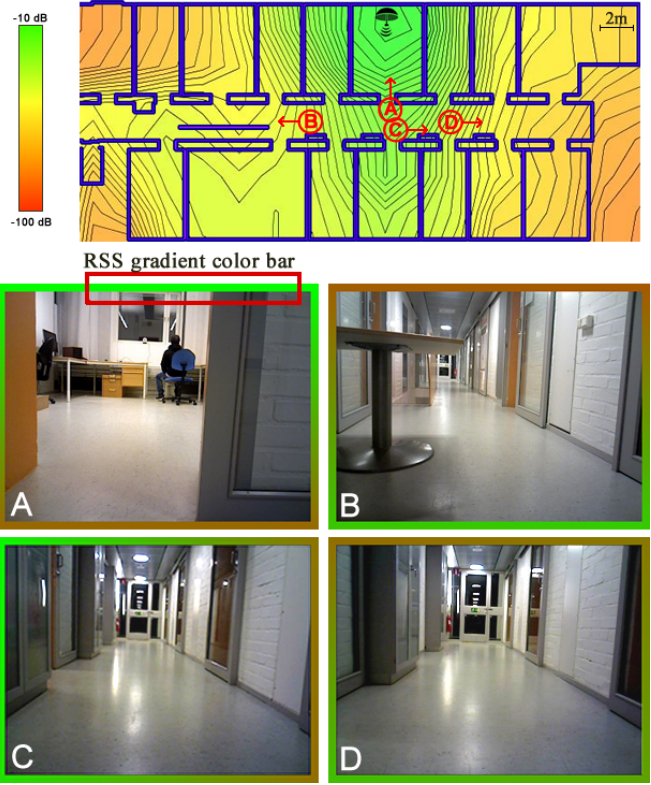


Fig. 4: Visualization of the RSS heat-map along with the robot locations and the view of the developed interface (HMI) at example positions (A-D). Arrows from A-D represents the camera's orientation. Note the green and red gradient, indicating higher and lower signal directions in the color bars surrounding the videos.

C. User Interface (HMI)

In a way that is similar to the way video games are controlled today, the operator HMI consists of a visual interface (monitor) providing a video feed from the robot during robot teleoperation. To provide visual feedback regarding the estimated DoA, we propose to use a rectangular border around the video feed, as illustrated in Fig 4.

The DoA estimates from Equation (4) are first mapped to the camera frame (by using the robot and camera orientations, and the FLC logic) and then translated to a color gradient, where a green color in the color bar indicates the higher signal strength direction, whereas a red color indicates a lower signal strength direction. Besides, the color intensity is scaled according to a linear interpolation of the measured RSS values. Thus the interface not only represents DoA but also gives a sense of the true RSS.

The code for estimating the DoA, generating the visual feedback, and also for the control mode, runs on the operator station, hence it does not increase the computational effort onboard the robot.

IV. EXPERIMENTAL EVALUATION

To verify the proposed approach, we performed two different experiments. The first experiment compares the accuracy of the DoA using the proposed directional antennas configuration with the omnidirectional configuration. The

second experiment investigates the usefulness of the proposed approach by verifying that the variation of the RSS along a robot path is indeed predicted by the DoA estimates.

A. Experimental setup

1) *Hardware*: For the experiments, we used a KUKA youBot equipped with an arm as shown in Figure 1. The video feed is provided by a PrimeSense camera, attached to the robot arm which acts as a pan-tilt system for the camera. A commercial Wi-Fi access point (AP) with a detachable external antenna is used as the radio signal source (transmitter). Five small USB wireless adapters of the same model (TP-Link TL-WN722N) with detachable external antennas are attached to the robot. These wireless adapters (WiFi stations) act as the radio receivers and are connected to the AP using the IEEE 802.11n 2.4 GHz channels. All connections are optimized for channel interference based on adjacent channels and unwanted networks in the environment.

Four wireless adapters (used for DoA estimate) connected to directional dish antennas (8 dBi) are placed at the robot's vertices as can be seen in Figures 1 and 2b. Here, the sensors' spatial separations are $\Delta_{SX} = 0.4m$, $\Delta_{SY} = 0.6m$. A fifth adapter (used for communication with the operator) is placed at the center and is connected to an external omnidirectional whip antenna (4 dBi).

For comparison with the DoA estimate using omnidirectional antenna configuration, we replaced the directional antennas with (external) omnidirectional whip antennas (4 dBi) and placed them on the robot as depicted in Figure 2a with $\Delta_{SX} = 0.4m$, $\Delta_{SY} = 0.4m$. In addition, we conducted the experiments with either omnidirectional whip (8 dBi) or directional dish (8 dBi) antennas at the AP with the transmit power fixed at 20 dBm. All the external antennas costed less than \$10 each.

2) *Environment*: It is well known that indoor environments are more challenging for wireless systems, in terms of e.g. multipath fading phenomena. Therefore we chose an office environment (400m²), including a hallway and a set of rooms, to perform our experiments. To get an overview of the RSS variations in the environment, we generated a heat-map of the RSS with fine measurements using a commercial wireless survey tool². The floor map along with the RSS heat-map is shown in the upper part of Figure 4. The hallway has 47cm thick concrete walls, while the walls in between offices are thinner and made of glass and plaster.

3) *Signal processing and HMI*: The FLC and the signal processing on the RSS are implemented in the Robot Operating System (ROS) framework. A laptop running Ubuntu 14.04, with a connected Xbox gamepad, is used for the teleoperation experiments. The laptop acts as the operator control station, provides the HMI to the operator and communicates with the robot through the wireless AP. The wireless adapters used in the study provide the RSS information using the

Received Signal Strength Indicator (RSSI³) metric, directly in terms of dBm. The RSSI is sampled at 5 Hz rate. As the RSS measurements are noisy, we applied an exponential moving average filter using the following model [12]:

$$\widehat{RSS}_i = RSS_{i-1} + \alpha(RSS_i - RSS_{i-1}), \quad (8)$$

to remove temporal fluctuations, where α is the smoothing parameter, set to 0.75 based on empirical tests. Following [23], we also applied a Moving Average Filter (MAF) to mitigate spatial multipath fading, with a window size equal to about 10λ (λ is the wavelength). For instance, at 0.2m/s velocity, 5Hz RSS sampling rate, and $\lambda = 12.5$ cm (at 2.4GHz), the MAF window size should be ≈ 30 to filter samples within 1.25m (10λ) displacement by the robot.

B. Experiments

1) *Antenna configurations*: The two configurations proposed in Section III-A are evaluated with both omnidirectional and directional antennas at the AP (transmitter) side, resulting in the following four combinations: Directional Tx (Transmitter) - Directional Rx (Receiver); Directional Tx - Omnidirectional Rx; Omnidirectional Tx - Directional Rx; and Omnidirectional Tx - Omnidirectional Rx. To evaluate which antenna configuration provides the best estimation of the DoA, we conducted several trials for each of the four configuration in LOS and NLOS conditions. The robot was placed at a fixed distance from the radio source and rotated following a pre-determined pattern, to ensure repeatability, with different velocities (0.1, 0.2 and 0.5 rad/s) taking measurements as can be seen in Figure 5.

2) *System evaluation*: Once the more appropriate antenna configuration is chosen, we performed a set of experiments aimed to evaluate the sensitivity, specificity, accuracy and precision of the network connectivity feedback information provided by the interface. The robot is teleoperated (at a velocity ≤ 0.2 m/s) for a random exploration task within the floor, simulating short missions, following different paths and trying to avoid low connectivity regions using the proposed interface. Eight different trials of this kind are conducted. In each trial, the transmitter is placed at different locations. An example trajectory made by the robot is shown in Figure 6. During each trial, we logged the robot odometry data (which is not very accurate as can be observed in Figure 6), the RSS data, the estimated DoA and the streamed video. A video illustrating the proposed method with an example trial is available⁴.

In a noise free world the following equality would hold:

$$\frac{dRSS}{dt} = \frac{dRSS}{dx} \frac{dx}{dt}. \quad (9)$$

The real world is however far from noise free, and we must experimentally verify that our estimates provide useful information to the human operator. We foresee that if the

³RSSI is a vendor-specific metric and therefore reports different values (or quantities) in different devices. The wireless adapters used in this paper reported reliable values of absolute signal power (dBm) as RSSI.

⁴<https://youtu.be/YcbP1c7eaQ>

²Ekahau site survey tool.

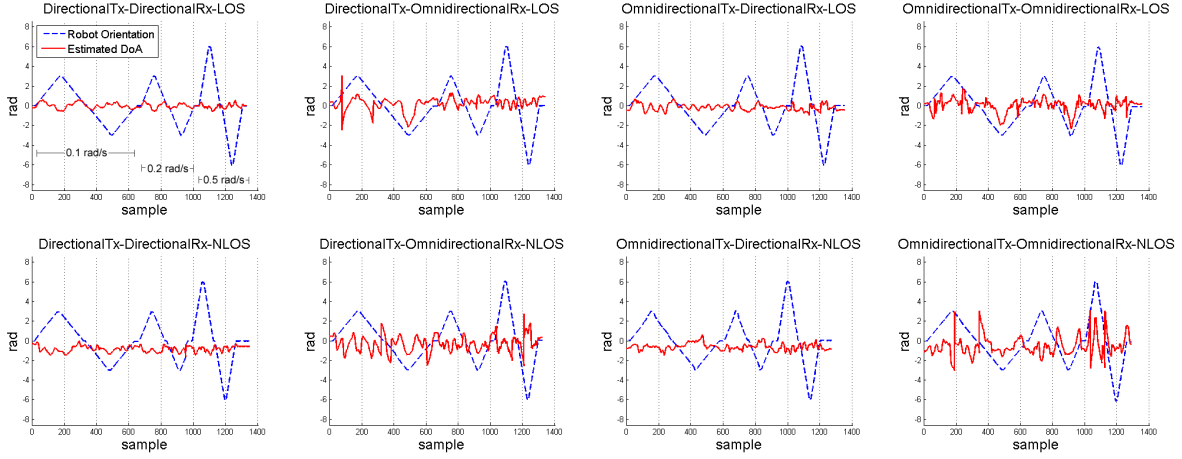


Fig. 5: DoA estimation results of the two configurations of receivers (shown in Figure 2) with directional transmitter (row 1) and omnidirectional transmitter (row 2). As can be seen, the use of directional receivers configuration (column 1 and 3) resulted in significantly less errors than omnidirectional receivers (column 2 and 4).

robot is moved in the direction of the estimated DoA, the measured RSS will increase. For this we used the RSS at

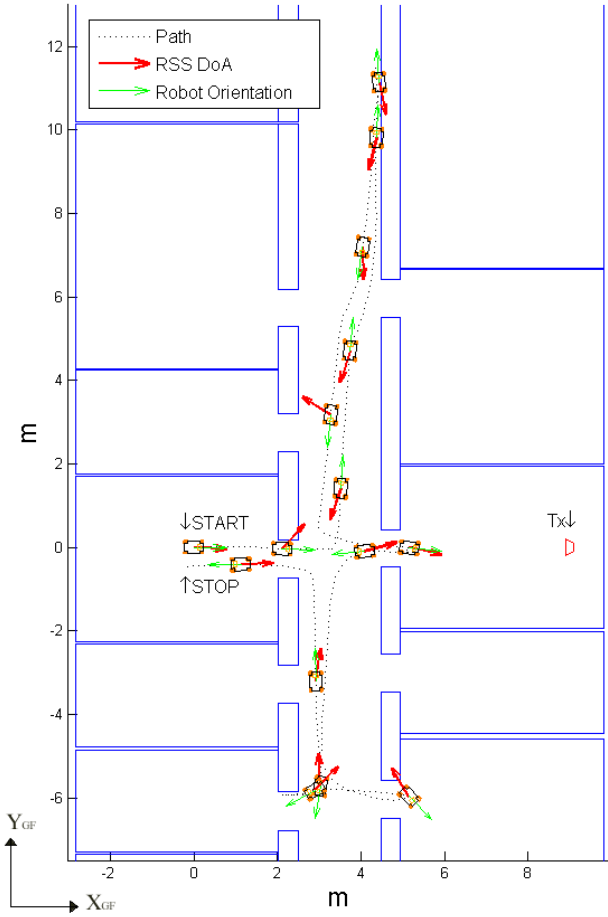


Fig. 6: Trajectory (downsampled) of the UGV in one of the experiments. The red arrows show the RSS DoA and the green arrows show the robot orientation in the global frame.

the central receiver to cross-verify the DoA obtained by the antennas on the vertices of the robot. We used finite differences in \overline{RSS}_C to estimate $\frac{dRSS}{dt}$, and \vec{V}_f as the estimate of $\frac{dRSS}{dx}$ and the odometer robot velocity $\vec{V}_{UGV}(t)$ to estimate $\frac{dx}{dt}$. The scalar (dot) product between the robot velocity and the computed RSS gradient \vec{V}_f at each instant is given by:

$$p(t) = \langle \vec{V}_f(t), \vec{V}_{UGV}(t) \rangle. \quad (10)$$

By comparing the scalar product $p(t)$ with the change in the RSS at the central receiver $\nabla_t RSS_C = \frac{dRSS_C}{dt}$, we can evaluate the proposed teleoperation system quantitatively. We expect a steep increase in RSS_C when $p(t)$ is positive and close to 1 (i.e. every time the user is moving towards the DoA). Similarly, we expect a sharp decrease in RSS_C when the $p(t)$ is negative and close to -1 (i.e. the user moves the robot away from the DoA).

V. RESULTS AND DISCUSSIONS

A. Antennas configurations

Figure 5 shows the results of the experiments with various antenna arrangements. Each plot shows the robot orientation (blue) and DoA of the RSS (red) in the global frame at each instant. We calculate the circular mean, $\bar{\phi} = \text{atan2}\left(\frac{\sum_{j=1}^n \sin \phi_j}{n}, \frac{\sum_{j=1}^n \cos \phi_j}{n}\right)$ and the circular standard deviation (STD) = $\sqrt{1 - \|\mathbf{r}\|}$, where $\mathbf{r} = \left[\frac{\sum_{j=1}^n \sin \phi_j}{n}, \frac{\sum_{j=1}^n \cos \phi_j}{n}\right]$. The reported angular mean, even though useful for comparison, does not account into the dynamics (temporal variations) of the DoA estimates, thereby the STD (or variance) predominates the analysis in this section. We expect the DoA to point toward the source (AP) or the highest RSS in the local region at every instant irrespective of the robot orientation.

Table I presents the results of the four antenna arrangements in a LOS condition. The expected DoA in these four cases is 0 rad (hence the estimated DoA also indicates the error in DoA estimation), which is the relative orientation

Transmitter	Receiver	Mean DoA (rad)	STD (rad)
Directional	Directional	0.02	0.19
Directional	Omnidirectional	0.26	0.41
Omnidirectional	Directional	-0.17	0.23
Omnidirectional	Omnidirectional	0.07	0.42

TABLE I: Transmitter placed in LOS. Expected DoA is 0 rad.

Transmitter	Receiver	Mean DoA (rad)	STD (rad)
Directional	Directional	-0.84	0.21
Directional	Omnidirectional	-0.34	0.52
Omnidirectional	Directional	-0.62	0.24
Omnidirectional	Omnidirectional	-0.70	0.56

TABLE II: Transmitter placed in NLOS. Expected DoA is ≈ -1 rad.

of the robot with respect to the source in the global frame. Table II reports the results for the NLOS condition, where the robot is fully blocked by a thick concrete wall in the hallway and is separated from the source with a distance of 6m with relative orientation of -1 rad.

In both LOS and NLOS, and for both directional and omnidirectional transmitter settings, the omnidirectional receivers configuration (column 2 and 4 of Figure 5) consistently provided noisy DoA estimates (with rapid variations around the mean value). In contrast, the directional receiver configurations (column 1 and 3 of Figure 5) exhibited lower variance (or STD) and better accuracy (mean error < 0.2 rad in LOS, < 0.4 rad in NLOS). This means that the directional receiver configuration (Figure 2b) produced reliable and stable DoA estimates at every instant, which is vital for a teleoperation system with DoA feedback. The results support the observations in [16] that the directional antennas are best suited for active tracking of the DoA.

Overall, the configuration “Directional Tx - Directional Rx” resulted in low variance with reasonably high accuracy. Hence we use this configuration for the next experiment to evaluate the whole teleoperation system with DoA feedback.

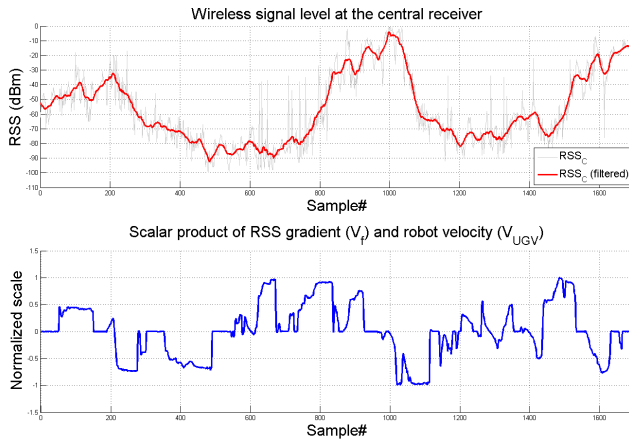


Fig. 7: Evaluation of the new UGV (robot) teleoperation FLC interface with wireless network connectivity perception.

B. System evaluation

Figure 7 shows the variations of RSS at the central receiver (RSS_C) and the scalar product $p(t)$ with time for the sample trial depicted in Figure 6. To quantify the system performances, we measure the number of true/false positives/negatives in the outcome. We define the *true positives* (TP) and *true negatives* (TN) as the number of occurrences where the user is driving in or away from the direction of the DoA while the RSS_C is increasing or decreasing respectively. Conversely, *false positives* (FP) and *false negatives* (FN) correspond respectively to the occurrences where the RSS_C is decreasing or increasing with the user’s movement towards or away from the DoA. The following equations show how they are calculated.

$$TP = \sum_{t=1}^N H(\nabla_t RSS_C(t))H(p(t) - \tau), \quad (11)$$

$$FP = \sum_{t=1}^N H(-\nabla_t RSS_C(t))H(p(t) - \tau), \quad (12)$$

$$TN = \sum_{t=1}^N H(-\nabla_t RSS_C(t))H(-(p(t) - \tau)), \quad (13)$$

$$FN = \sum_{t=1}^N H(\nabla_t RSS_C(t))H(-(p(t) - \tau)), \quad (14)$$

where $\nabla_t RSS_C(t) = \frac{RSS_C(t+1) - RSS_C(t)}{T_s}$ with T_s being the RSS sampling interval, N is the number of samples analyzed, H is a unit step function (output is 0 for negative arguments and 1 for positive arguments), and τ is a threshold set to avoid zeros in the scalar product (explained later).

From these definitions, we compute Sensitivity ($\frac{TP}{TP+FN}$), Specificity ($\frac{TN}{FP+TN}$), Precision ($\frac{TP}{TP+FP}$), and Accuracy ($\frac{TP+TN}{TP+TN+FP+FN}$) metrics. The threshold value ($\tau \in \mathcal{R}^+$) is used to remove static measurements (where $p(t)$ is equal or close to 0) and to alleviate minute odometer errors such as a small linear velocity generated during a rotation in place (which empirically determines the value of τ).

It can be seen in Figure 6 that the estimated DoA sometimes pointed towards the corridor or the doorways (instead of the true source location). This is expected because of substantial exposure of radio signals from these regions. Table III shows the results obtained for the experiments conducted on different teleoperation missions as explained in the Section IV-B.2. The proposed system delivered 82%

Mission	Sensitivity	Specificity	Precision	Accuracy
1 (5.6 min)	0.87	0.79	0.78	0.83
2 (14.2 min)	0.70	0.85	0.82	0.77
3 (10.7 min)	0.67	0.76	0.72	0.72
4 (10.0 min)	0.81	0.82	0.81	0.82
5 (11.1 min)	0.81	0.90	0.87	0.86
6 (11.4 min)	0.72	0.87	0.88	0.78
7 (5.0 min)	0.70	0.76	0.80	0.72
8 (5.5 min)	0.62	0.90	0.86	0.76
Mean	0.74	0.83	0.82	0.78

TABLE III: Evaluation of the system with sensitivity, specificity, precision and accuracy for different sorties, calculated with MAF window size = 30 and $\tau = 0.1$.

precision and 78% accuracy in guiding the teleoperator with network connectivity feedback in an indoor environment. As the analysis depend on the UGV's velocity from the odometer, we presume that odometry errors could have contributed to reduced accuracy of the proposed system. Thus a better localization technique will improve the overall system accuracy. The main limitations in the proposed solution are the physical constraints on the robot and reliability of the RSS readings. Note that the system is also reasonably sensitive (74%) in directing the operator into high wireless signal regions (towards DoA) while maintains high specificity (83%) in pointing out low-wireless signal regions.

Although the quantitative results presented in this paper are assuring, qualitative evaluation with user studies are nevertheless required to demonstrate the effectiveness of the new interface with human in the loop. This forms a basis of our future work. Additionally, the directional antennas used in this study can also be exploited for communication redundancy, offering advantages such as increased coverage, stable connections, and coverage in elevated regions [15].

VI. CONCLUSIONS

We looked at the possibility of providing a visually intuitive interface for presenting the network connectivity information with directionality at the HMI for naturally guiding the human operators to drive a mobile robot (UGV) into high wireless coverage regions and avoid low-wireless signal regions. We integrated this system with a novel Free Look Control (FLC) mode which provides a first person view of the surroundings from the robot camera, in a way that is similar to a First Person Shooter (FPS) computer game.

We proposed a spatial-diversity based technique with multiple directional wireless receivers to accurately estimate the radio signal strength (RSS) direction of arrival (DoA). We compared our proposed DoA estimation method with finite difference method using omnidirectional antennas and demonstrated that the DoA estimates using directional receivers resulted in high accuracy (mean error < 0.4 rad even in NLOS). Finally, we conducted experiments to objectively validate the proposed interface and have demonstrated high reliability and precision ($\approx 82\%$) in providing useful network connectivity information to the operator.

We believe that these results will provide a significant contribution towards creating a HMI where the operator situational awareness includes not only spatial components, but also network connectivity information, thus enabling better performance in time-critical robotic missions such as urban search and rescue.

REFERENCES

- [1] K. Nagatani, S. Kiribayashi, Y. Okada, S. Tadokoro, T. Nishimura, T. Yoshida, E. Koyanagi, and Y. Hada, "Redesign of rescue mobile robot Quince," in *IEEE International Symposium on Safety Security and Rescue Robotics*. IEEE, 2011, pp. 13–18.
- [2] J. Casper and R. R. Murphy, "Human-robot interactions during the robot-assisted urban search and rescue response at the World Trade Center," *IEEE Transactions on Systems, Man and Cybernetics, Part B (Cybernetics)*, vol. 33, no. 3, pp. 367–385, 2003.
- [3] M. Lindhè, K. H. Johansson, and A. Bicchi, "An experimental study of exploiting multipath fading for robot communications," in *Proceedings of Robotics: Science and Systems*, June 2007.
- [4] A. Birk and H. Kenn, "A rescue robot control architecture ensuring safe semi-autonomous operation," *RoboCup 2002. Robot Soccer World Cup VI*, 2003.
- [5] T. Fong and C. Thorpe, "Vehicle teleoperation interfaces," *Autonomous robots*, vol. 11, no. 1, pp. 9–18, 2001.
- [6] R. Wegner and J. Anderson, "Agent-Based Support for Balancing Teleoperation and Autonomy in Urban Search and Rescue," *International Journal of Robotics and Automation*, vol. 21, no. 2, pp. 1–19, 2006.
- [7] J. Burke, R. Murphy, M. Covert, and D. Riddle, "Moonlight in Miami: An ethnographic study of human-robot interaction in USAR," *Human-Computer Interaction, special issue on Human-Robot Interaction*, vol. 19, pp. 1–2, 2004.
- [8] H. Yanco and J. Drury, "Where Am I? Acquiring Situation Awareness Using a Remote Robot Platform," *IEEE Conference on Systems, Man and Cybernetics*, 2004.
- [9] J. L. Drury, J. Scholtz, and H. A. Yanco, "Awareness in human-robot interactions," in *IEEE International Conference on Systems, Man and Cybernetics*, vol. 1. IEEE, 2003, pp. 912–918.
- [10] P. Ögren, P. Svenmarck, P. Lif, M. Norberg, and N. E. Söderbäck, "Design and Implementation of a New Teleoperation Control Mode for Differential Drive UGVs," *Autonomous Robots*, 2014.
- [11] A. Owen-Hill, R. Parasuraman, and M. Ferre, "Haptic teleoperation of mobile robots for augmentation of operator perception in environments with low-wireless signal," in *IEEE International Symposium on Safety, Security, and Rescue Robotics (SSRR)*, Oct. 2013.
- [12] R. Parasuraman, T. Fabry, L. Molinari, K. Kershaw, M. D. Castro, A. Masi, and M. Ferre, "A Multi-Sensor RSS Spatial Sensing-Based Robust Stochastic Optimization Algorithm for Enhanced Wireless Tethering," *Sensors*, vol. 14, no. 12, pp. 23 970–24 003, 2014.
- [13] K. Gkikas, "The evolution of FPS games controllers: how use progressively shaped their present design," in *Panhellenic Conference on Informatics (PCI)*, 2007.
- [14] H. A. Yanco and J. L. Drury, "Rescuing interfaces: A multi-year study of human-robot interaction at the AAAI Robot Rescue Competition," *Autonomous Robots*, vol. 22, no. 4, pp. 333–352, 2007.
- [15] Y. Hada and O. Takizawa, "Development of communication technology for search and rescue robots," *Journal of the National Institute of Information and Communications Technology*, vol. 58, no. 1, 2011.
- [16] B.-C. Min, E. Matson, and B. Khaday, "Design of a networked robotic system capable of enhancing wireless communication capabilities," in *IEEE International Symposium on Safety, Security, and Rescue Robotics (SSRR)*, Oct 2013.
- [17] N. Bezzo, B. Griffin, P. Cruz, J. Donahue, R. Fierro, and J. Wood, "A cooperative heterogeneous mobile wireless mechatronic system," *IEEE/ASME Transactions on Mechatronics*, vol. 19, no. 1, pp. 20–31, Feb. 2014.
- [18] D. Han, D. Andersen, M. Kaminsky, K. Papagiannaki, and S. Seshan, "Access point localization using local signal strength gradient," in *Passive and Active Network Measurement*, ser. Lecture Notes in Computer Science, S. Moon, R. Teixeira, and S. Uhlig, Eds. Springer Berlin Heidelberg, 2009, vol. 5448, pp. 99–108.
- [19] J. N. Twigg, J. R. Fink, P. Yu, and B. M. Sadler, "RSS gradient-assisted frontier exploration and radio source localization," in *IEEE International Conference on Robotics and Automation (ICRA)*. IEEE, 2012, pp. 889–895.
- [20] S. Venkateswaran, J. T. Isaacs, B. M. Sadler, J. P. Hespanha, and U. Madhow, "RF source-seeking by a micro aerial vehicle using rotation-based angle of arrival estimates," in *Proc. of the 2013 Amer. Contr. Conf.*, June 2013.
- [21] R. Parasuraman, T. Fabry, K. Kershaw, and M. Ferre, "Spatial sampling methods for improved communication for wireless relay robots," in *International Conference on Connected Vehicles and Expo (ICCVE)*. IEEE, Dec. 2013, pp. 874–880.
- [22] C. Shannon, "Communication in the presence of noise," *Proceedings of the IRE*, vol. 37, pp. 10–21, 1949.
- [23] R. Valenzuela, O. Landron, and D. Jacobs, "Estimating local mean signal strength of indoor multipath propagation," *IEEE Transactions on Vehicular Technology*, vol. 46, no. 1, pp. 203–212, Feb 1997.